

---

# THREE-DIMENSIONAL NUMERICAL SIMULATION OF A CONTINUOUSLY ROTATING DETONATION IN THE ANNULAR COMBUSTION CHAMBER WITH A WIDE GAP AND SEPARATE DELIVERY OF FUEL AND OXIDIZER

---

**S. M. Frolov, A. V. Dubrovskii, and V. S. Ivanov**

Center of Pulse Detonation Combustion  
Semenov Institute of Chemical Physics  
4 Kosygin Str., Moscow 119991, Russia

The possibility of integrating the Continuous Detonation Chamber (CDC) in a gas turbine engine (GTE) is demonstrated by means of three-dimensional (3D) numerical simulations, i. e., the feasibility of the operation process in the annular combustion chamber with a wide gap and with separate feeding of fuel (hydrogen) and oxidizer (air) is proved computationally. The CDC with an upstream isolator damping pressure disturbances propagating towards the compressor is shown to exhibit a gain in the total pressure of 15% as compared with the same combustion chamber operating in the deflagration mode.

## 1 INTRODUCTION

Modern power plants in aircraft are mainly GTEs utilizing Brayton thermodynamic cycle. A similar (constant-pressure combustion) cycle is widely used in liquid rocket engines (LREs). For many decades, GTEs and LREs were continuously improved and further improvement requires large capital investments. An alternative solution to significantly improve the thermodynamic efficiency of modern GTEs and LREs is the use of the combustion chambers with the total pressure gain. Increasing the total pressure in the combustion chamber can be provided by an increase in the burning rate of a mixture of fuel with the oxidant and/or by changing the combustion mode. The most attractive combustion mode in terms of its thermodynamic efficiency is the detonation [1, 2]. In a detonation wave, the chemical energy stored in the fuel is released with the extremely high rate in a very thin layer of shock-compressed mixture. There are two



**Figure 1** Architecture of the GTE operating on continuously rotating detonations

basic schemes of detonation combustion: in periodic detonation waves traveling along the combustion chamber (pulse detonation chambers, PDCs [3, 4]) and in a detonation wave continuously circulating in a tangential direction across the combustion chamber (CDCs [2, 5, 6]). These schemes are currently considered promising for both air-breathing and rocket engines [5–15].

In 2010, the Centre for Pulse Detonation Combustion at Semenov Institute of Chemical Physics of the Russian Academy of Sciences launched an ambitious project aimed at developing scientific grounds for designing CDCs for power engineering and aerospace applications. The project implied the development of the computer code that allows full-scale 3D simulation of the operation process in CDCs of different design.

In [11, 14], with this code the operation process in the annular CDC operating on the homogeneous stoichiometric hydrogen–air mixture fed through the injector head with two annular openings of relatively small width ( $\sim 7$  mm) was thoroughly investigated. It was shown that the CDC is the combustion chamber with the total-pressure gain: in the calculations, the total pressure in the chamber was increased by 10%–14%. The calculations of [11, 14] were mainly focused on the flow characteristics in the input and output devices of the CDC referred to as upstream and downstream isolators separating the CDC from the compressor and turbine of the GTE, respectively (Fig. 1). It turned out that the chosen annular geometry of the upstream and downstream isolators did not provide proper damping of pressure disturbances generated by the detonation once they reach the GTE compressor and turbine. The estimated amplitudes of the pressure disturbances after passing the isolators attained very high values of 40%–45%  $P_{in}$  and 30%–35%  $P_{in}$ , respectively, where  $P_{in}$  is the pressure behind the last stage of the GTE compressor.

In [15], a 3D numerical simulation of the operation process in an annular CDC with separate supply of fuel components — hydrogen and air — was performed. The design of the CDC and the main operational parameters were the same as in experiments [5, 6]. The air was fed to the chamber axially through the 2-millimeter wide annular gap, whereas hydrogen was fed through multiple radial holes of submillimeter size equally distributed along the circumference of the outer CDC wall. The calculations took into account the effects associated with the finite rates of molecular and turbulent mixing of fuel components with each other and with the detonation products, and with the finite rates of chemical transformations. The calculation results were shown to be generally consistent with the experimental observations in terms of all the integral characteristics of

the operation process (mean static pressure in the CDC, mass flow rates of fuel components, the height of the detonating layer, etc.).

This article is the continuation of studies [11, 14, 15]. The objective of the present work is to prove the feasibility of integrating the CDC into the GTE, i. e., to prove the possibility of arranging the operation process in an annular CDC with a wide gap (comparable to the height of the last stage of the GTE compressor blades) with separate supply of fuel and oxidizer.

## 2 PROBLEM FORMULATION

Figure 2 shows the schematic of the CDC with an annular gap of width  $\delta = 23$  mm equipped with the upstream isolator in the form of the expansion chamber with the maximum width  $\Delta$ . The outer diameter of the CDC is 306 mm. The detailed design of the isolator is a subject of patent [16] and is not discussed here. Oxidant (air) under static pressure  $P_{in}$  and temperature  $T_{in}$  is fed in the CDC through the isolator axially. Fuel (hydrogen) is supplied to the CDC from the fuel reservoir (not shown in Fig. 2) through 80 radial injector bores: 40 in the outer wall and 40 in the inner wall. Pressure and temperature of hydrogen in the fuel reservoir are kept constant and equal to  $P_f$  and  $T_f$ , respectively. Downstream of the CDC, a provision is made for a divergent nozzle formed by a conical central body (cone half-angle is  $10^\circ$ ) and a large buffer volume (not shown in Fig. 2) exceeding considerably the volume of the chamber and used for avoiding parasitic numerical reflections.

The main tasks attacked in this work are: (i) to design the CDC ensuring continuous detonative combustion with an appreciable gain in total pressure and (ii) to design the upstream isolator of the CDC which could provide effective damping of pressure disturbances propagating towards the GTE compressor.

The physicochemical processes in the CDC are simulated using the mathematical model described in detail in [11]. Here, the authors limit themselves to

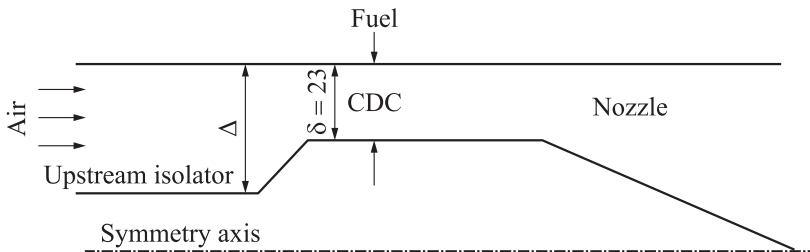
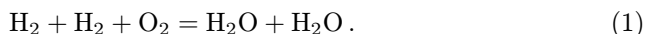


**Figure 2** Schematic of the annular CDC with the upstream isolator, radial fuel injectors, and a nozzle. Dimensions are in millimeters

a brief description of its main features. The flow of a viscous compressible gas in the CDC is described using the 3D unsteady Reynolds-averaged Navier–Stokes (URANS), energy, and species conservation equations for a multicomponent mixture. The turbulent fluxes of species, momentum, and energy are modeled within the framework of the standard  $k$ – $\varepsilon$  turbulence model for a compressible flow. Given that all physicochemical processes in the CDC occur in a very short time, the contribution from the frontal (laminar and/or turbulent) combustion to the chemical sources in the equations of conservation of energy and components of the mixture is neglected. The contributions of these reactions to the bulk (volumetric) chemical sources are determined using the particle method (PM) [11]. The most important advantage of the PM is its ability to accurately determine the rates of chemical reactions in a turbulent flow without invoking any hypothesis about the influence of turbulent fluctuations of the temperature and concentrations of the reactants on the mean rate of the reaction. In the PM algorithm, the instantaneous local states of a turbulent reacting flow are represented as a set of interacting (Lagrangian) particles. Each particle has its individual properties: the position in space, three velocity components, volume, density, temperature, mass fractions of chemical species, and statistical weight, which is used to determine the mean values of the variables over the ensemble of particles. For each particle, the system of equations of conservation of mass of the species, momentum, and energy is solved; the flux (transport) terms are calculated using the classic models of linear relaxation to the mean [17]. The equations of the model are closed by the caloric and thermal equations of state of a mixture of ideal gases with variable specific heats, as well as by the initial and boundary conditions. All the thermophysical parameters of the gas are considered variable.

Numerical solution of the governing equations of the problem is carried out using the coupled algorithm “Semiimplicit method for pressure linked equations (SIMPLE)–Monte Carlo method.” The chemical sources are calculated by an implicit scheme with internal time stepping. The coupled algorithm was previously used to simulate flame acceleration and deflagration-to-detonation transition in smooth tubes and in tubes with obstacles [18, 19], as well as to solve the problems of shock-initiated autoignition and preflame ignition in confined spaces [20]. In all cases, satisfactory agreement between the results of calculations and experiments were observed. In addition, this algorithm was used to solve the problem of the limits of existence of detonation in the CDC operating on homogeneous hydrogen–air mixture. As in [11, 14, 15], the oxidation of hydrogen was described by a single-step reaction scheme:



The rate of hydrogen oxidation at elevated pressures  $P$  (5 to 40 atm) and temperatures  $T$  (1100–2000 K) was calculated by the formula:

$$\left[ \dot{\text{H}}_2 \right] = -8 \cdot 10^{11} P^{-1.15} [\text{H}_2]^2 [\text{O}_2] e^{-10^4/T} \quad (\text{atm, mol, L, s}) \quad (2)$$

where  $P$  is the pressure and  $[S]$  denotes the concentration of species  $S$ . Equation (2) was obtained by fitting the dependences of the induction period on the pressure and temperature obtained for reaction (1) to those calculated within the framework of an extensively tested detailed kinetic mechanism of hydrogen oxidation [21, 22]. Note that the heat of reaction (1) was modified to make the calculated Chapman–Jouguet detonation velocity  $D_{CJ}$  for the stoichiometric hydrogen–air mixture be consistent with its thermodynamic value ( $D_{CJ} \approx 1970$  m/s).

The boundary conditions for the average flow velocity, pressure, temperature, turbulent kinetic energy and its dissipation rate, and mean concentrations of chemical species on the solid walls of the CDC are set using the formalism of wall functions on the assumption that the walls are isothermal ( $T_w = 293.15$  K), impermeable, and noncatalytic, with noslip properties.

The inlet boundary conditions in air and hydrogen reservoirs are taken in the form of fixed values of the pressure, temperature, turbulent kinetic energy and its dissipation rate, as well as fixed values of the average concentrations of oxidant and fuel, respectively.

At the boundaries of the buffer volume attached to the CDC nozzle, the von Neumann condition,  $\text{grad}(P) = 0$ , is set. The rest of the variables (velocity, temperature, turbulent kinetic energy and its dissipation rate, and the concentrations of components) are extrapolated to these boundaries from the computational domain. Special calculations demonstrated that the specified boundary conditions at the buffer volume boundaries produce no effect whatsoever on the solution.

The boundary conditions for the particles (the components of the velocity vector and scalar variables) on the solid walls of the CDC and the open boundaries of the computational domain are formulated in such a way that they are consistent with the boundary conditions for the mean values of the relevant variables. This consistency is continuously monitored by comparing the values of the variables obtained by averaging over the ensemble of particles in the computational mesh with the average values of the same variables obtained by solving the averaged flow equations.

The initial conditions for the average parameters of the flow are formulated as follows. It is assumed that at initial time  $t = 0$ , the air and hydrogen reservoirs are filled with air and hydrogen under static pressures  $P_{in}$  and  $P_f$ , respectively, and the rest of the region is filled with quiescent air at atmospheric pressure.

The initial positions of the particles in the computational domain are selected using a random number generator capable of providing an on-average uniform distribution over a unit-length interval. At the initial time, each particle is characterized by a set of specific values of all relevant variables consistent with the initial distributions of the corresponding average values. The nominal number of particles in the computational mesh is specified before simulation,  $N_p = 10$ . Note that in the process of computations, the actual number of particles in the meshes

can change (particles migrate over the computational domain). To keep the number of particles unchanged, special procedures of cloning and clustering are applied. The pattern of the flow in the CDC is generally dependent on the chosen value of  $N_p$  and on the computational grid. However, previous calculations in [11, 14, 15] showed that at  $N_p > 10$ –15, the dependence of the flow pattern on  $N_p$  becomes weak. The influence of the computational grid was investigated by comparing the results of calculations on different grids.

The calculation procedure is started with purging the CDC for 0.4 ms, a time long enough to form a 10-centimeter thick active layer of hydrogen–air mixture over the plane of hydrogen injectors. Then, the procedure of detonation initiation is performed. This procedure amounts to a rapid burning of particles located in the initiator region, a limited-size area in the active layer. The combustion of the particles rapidly raises the pressure in the initiator region, thereby forming a shock wave. To ensure the propagation of the detonation wave in the desired direction, for example, counterclockwise, the initial distribution of particles in the CDC in the clockwise direction from the initiator region contains a layer of temporarily inert particles. Immediately after the initiation of detonation, these particles become active.

The calculations are performed on structured grids with hexagonal cells ranging in size from 0.5 to 2 mm. Despite the fact that such computational grids do not resolve the internal structure of the detonation front, the use of the PM takes into account the influence of longitudinal and transverse acoustic waves on chemical reactions inside the computational cell. The integration time step does not exceed 1  $\mu$ s.

### 3 RESULTS

Table 1 lists the calculation conditions used in this study and indicates the resultant combustion modes.

As mentioned above, initiation of detonation in the CDC is preceded by purging the chamber with fuel components. Figure 3 shows the successive distributions of hydrogen mass fraction in the CDC cross section located at an axial distance of 50 mm downstream from the hydrogen injectors during first 180  $\mu$ s of purging in Run 1 (see Table 1). It can be seen that by about 120  $\mu$ s, the mean hydrogen mass fraction in this cross section is close to stoichiometric (0.028), but the mixture is periodically stratified: mixture layers enriched with fuel are interspersed with fuel-lean layers.

About 3–4 ms after the detonation initiation, a periodic operation mode with a transverse detonation wave propagating continuously in the annular gap at the average velocity of  $\sim 1850$  m/s is established in the CDC in Run 1 (referred to as “continuous detonation” mode in Table 1). The settled frequency of detonation rotation in the chamber is approximately equal to 2 kHz.

**Table 1** Calculation conditions and the resultant combustion modes

Run	$P_{in}$ , atm	$T_{in}$ , K	$P_f$ , atm	$T_f$ , K	$\Delta$ , mm	Combustion mode
1	9	550	27	298	90	Continuous detonation
2	9	550	36	298	90	Continuous detonation with much unburned fuel
3 <sup>a</sup>	9	550	27	298	90	Stabilized deflagration
4	13	600	36	298	90	Stabilized deflagration
5	7	460	18	298	90	Stabilized deflagration
6	9	550	23	298	90	Detonation blow-off
7	7	460	36	298	90	Detonation blow-off
8	7	460	27	298	90	Continuous detonation
9	7	460	27	298	45	Continuous detonation

<sup>a</sup>Mixture is ignited by a hot ignition source all throughout the area over hydrogen injectors.

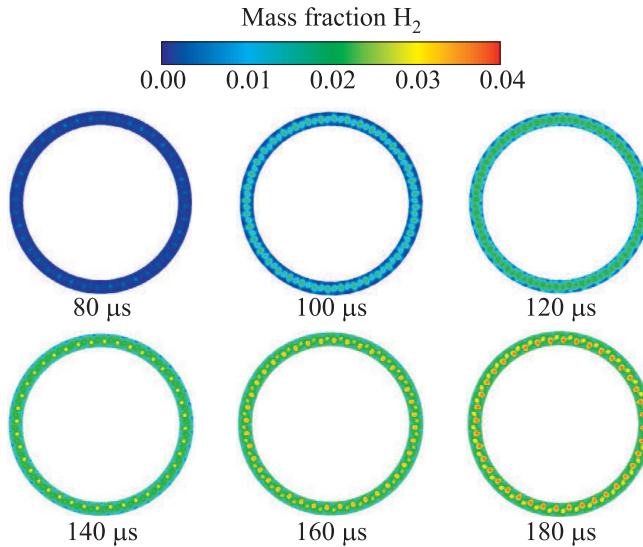


**Figure 3** Instantaneous distributions of hydrogen mass fraction in the CDC cross section at the stage of chamber filling with fuel components before detonation initiation in Run 1

Figure 4 shows the calculated instantaneous static pressure (Fig. 4a) and temperature (Fig. 4b) distributions in the vicinity of the CDC outer wall in the periodic operation mode with a single detonation wave (Run 1). Detonation propagates from right to left. It is seen that the hydrogen-air mixture ahead of

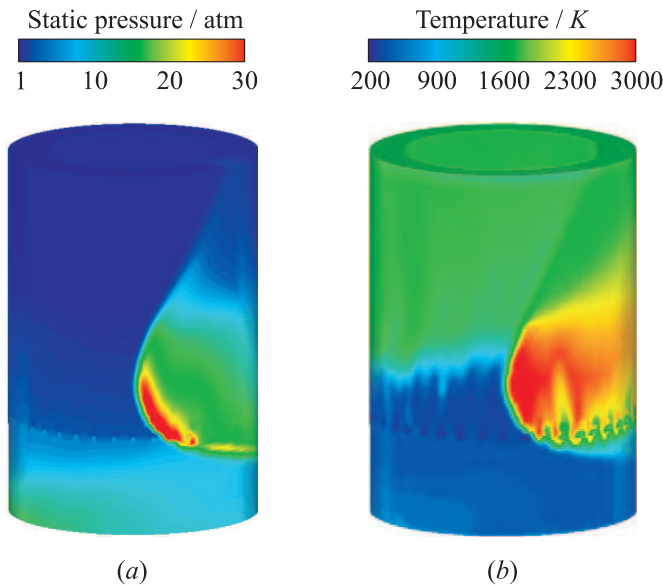


**Figure 4** Instantaneous distributions of static pressure (*a*) and temperature (*b*) near the outer wall of the CDC operating in the continuous detonation mode in Run 1. Detonation propagates from right to left

the detonation wave is periodically stratified not only in terms of the composition (see Fig. 3), but also in terms of temperature (see Fig. 4*b*), as air enters the upstream isolator with temperature 550 K and hydrogen, expanding into the injector holes, is cooled to a temperature of  $\sim 200$  K. In addition to the periodic stratification of the mixture in terms of temperature and composition in the CDC cross section, the calculations show a substantial variation in the temperature and composition of the hydrogen–air mixture in the axial direction: along the mixture layer ahead of the detonation wave. For this reason, the detonation wave possesses a highly curved front with its upper part displaced ahead of its lower part by about  $2\delta$  and with the apparent front height of approximately  $4.5\delta$  ( $\sim 100$  mm). A very similar continuous detonation mode is obtained in Run 2 (see Table 1) but a large amount of unburned hydrogen exists at the CDC outlet due to a highly fuel-rich overall mixture composition.

For the sake of comparison, Figs. 5 and 6 show the calculated instantaneous static pressure (see Fig. 5*a*) and temperature (see Figs. 5*b* and 6) distributions in the vicinity of the outer wall under conditions of stabilized deflagration (diffusion combustion) in the same annular chamber (Runs 3 and 4 in Table 1). In Run 3 (see Fig. 5), with the same calculation conditions as in Run 1, the stabilized deflagration rather than continuous detonation mode is readily obtained

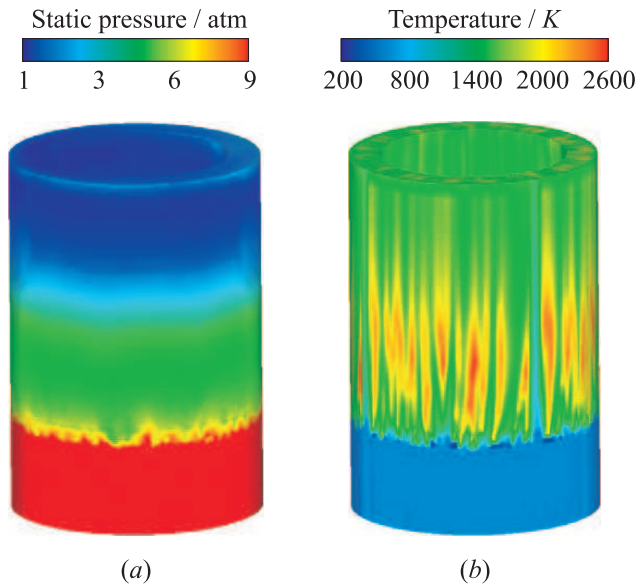


**Figure 5** Instantaneous distributions of static pressure (*a*) and temperature (*b*) near the outer wall of the CDC operating in the stabilized deflagration mode in Run 3

by igniting the mixture evenly by a hot ignition source all throughout the area over hydrogen injectors. In Run 4 (see Fig. 6), the deflagration mode is obtained in the course of process evolution as a result of detonation failure and gradual establishment of the stabilized deflagration mode. A similar system evolution was observed in Run 5. In the stabilized deflagration mode, combustion covers the entire cross section of the chamber and the static pressure and temperature decrease monotonically toward the nozzle.

Runs 6 and 7 in Table 1 represent the limiting conditions of CDC operation. In these Runs, the detonation wave once initiated is blown off from the CDC without further establishment of the stabilized deflagration mode.

Among all the combustion modes observed in the calculations, the continuous detonation mode of Run 1 is of most interest. Therefore, this mode is considered here in more detail. Figure 7 shows the calculated time histories of the static pressure at two points in the CDC: at a point located 50 mm above hydrogen injectors (solid curve) and at a point in the upstream isolator with  $\Delta = 90$  mm (dashed curve). It is seen that the static pressure in the CDC is pulsating with the maximum and minimum values attaining 30–35 and 3–4 atm, respectively. Taking the average of the solid curve in Fig. 7 gives the average static pressure in the CDC of  $\sim 8.6$  atm, which is somewhat lower (by 4.4%) than the inlet air

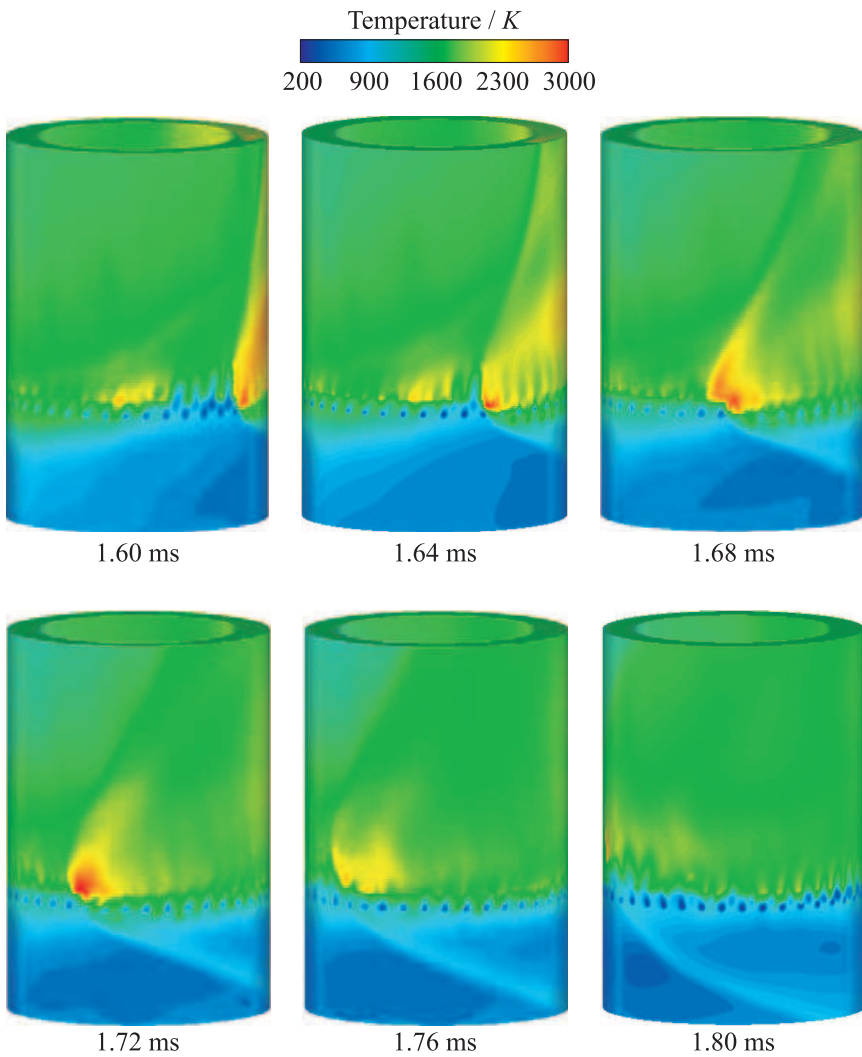


**Figure 6** Transition from detonation to stabilized deflagration mode in Run 4

pressure  $P_{in}$ . Nevertheless, as shown below, the CDC exhibits a gain in the total pressure.

One of the most important results of this work is the proof that using the upstream isolator of specific design, one can ensure almost complete damping of pressure disturbances propagating upstream from the CDC towards the last

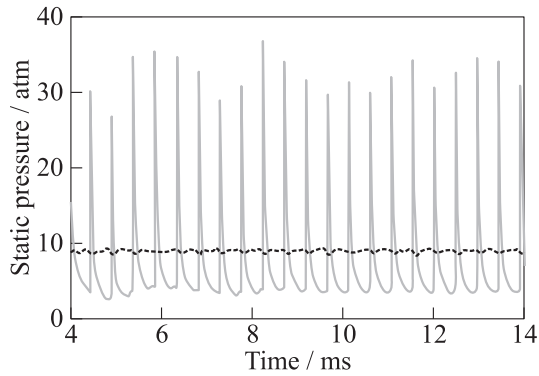


**Figure 7** Predicted time histories of static pressure in the middle of the CDC (solid curve) and in the upstream isolator with  $\Delta = 90$  mm (dashed curve)

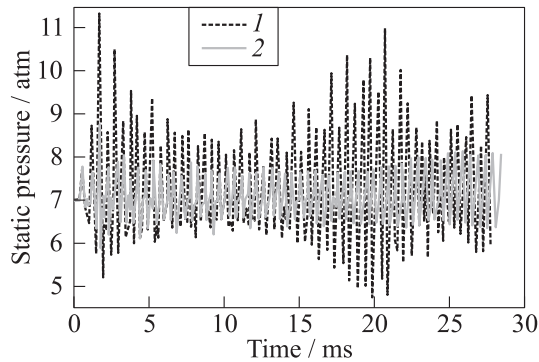


**Figure 8** Predicted time histories of static pressure in the upstream isolators of different width: 1 —  $\Delta = 45$  mm; and 2 —  $\Delta = 90$  mm

stage of the GTE compressor. Indeed, the maximum deviation of the dashed curve from the straight line in Fig. 7 is only 3%  $P_{in}$ .

Runs 8 and 9 in Table 1 demonstrate the effect of the isolator width  $\Delta$  on its damping efficiency. As is seen in Fig. 8, the decrease in the isolator width  $\Delta$  from 90 to 45 mm results in deterioration of the isolator damping efficiency: at  $P_{in} = 7$  atm, the amplitude of pressure disturbances in the isolator changes from 1–1.5 atm (14%–21%  $P_{in}$ ) at  $\Delta = 90$  mm to 2–6 atm (29%–86%  $P_{in}$ ) at  $\Delta = 45$  mm.

Figure 9 compares the calculated distributions of the cross-section-averaged total pressure along the CDC operating in the continuous detonation mode of Run 1 (solid curve) and that in the stabilized deflagration mode of Run 3 (dashed

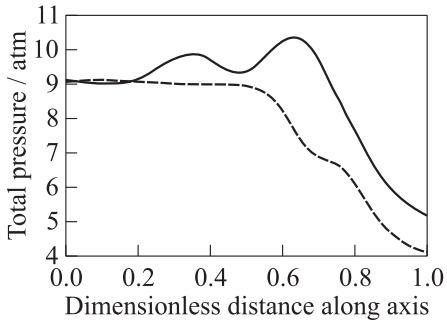


**Figure 9** Estimated distribution of the total pressure averaged over the cross section in the annular combustion chamber with detonation (solid curve, Run 1) and deflagration (dashed curve, Run 3)

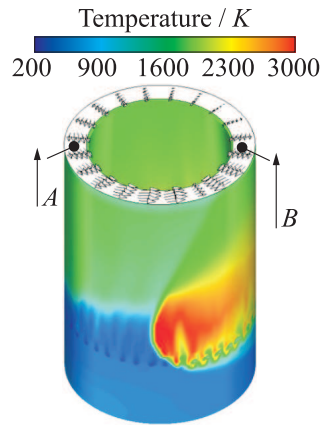


**Figure 10** Predicted flow pattern at the CDC exit in Run 1. The lengths of the vectors *A* and *B* in the corresponding points represent the scale for the longitudinal velocity component (*A*: 1470 m/s; and *B*: 1610 m/s). Transverse velocity components have the same scale

curve). The cross-section averaged total pressure  $p^*$  for the quasi-stationary periodic flow was determined as

$$p^* = \overline{p + \rho U^2} = \frac{1}{\Delta t} \int_{\Delta t} \frac{\sum_i (p_i + \rho_i U_i^2) \rho_i V_i}{\sum_i \rho_i V_i} dt$$

where  $p$  is the static pressure;  $\rho$  is the density;  $U$  is the length of the velocity vector;  $V$  is the volume;  $\Delta t$  is the detonation rotation time period; and index  $i$  denotes the computational cell number in the chosen cross section. It is seen from Fig. 9 that unlike the deflagration mode in which the total pressure gradually decreases along the axis of the chamber, the detonation mode exhibits the increase in the total pressure to 10.3 atm, i. e., is higher than  $P_{in}$  by about 15%. This is another important result of the present study.

One more interesting result is depicted in Fig. 10 demonstrating the velocity field at the CDC exit. It follows from Fig. 10 that the transverse flow direction at the CDC exit is opposite to the direction of detonation propagation due to specific pressure distribution in the annular combustion chamber with a continuously rotating detonation wave. As a matter of fact, in Fig. 10, the detonation wave propagates in the clockwise direction (for the observer at the CDC top), whereas the flow ahead of the detonation wave is directed counterclockwise.

It is also seen that the transverse velocity component is considerably smaller than the axial one with the latter exceeding the local sound velocity.

## 4 CONCLUDING REMARKS

The possibility of arranging a cyclic operation in the detonation mode of the CDC with a wide annular gap (23 mm) comparable to the height of the blades of the last stage GTE compressor and with separate delivery of fuel and oxidizer has been demonstrated computationally based on 3D URANS simulations coupled with the Particle method modeling micromixing and turbulence–chemistry interaction. A 15 percent gain in total pressure has been obtained in the CDC. A proposed design of the upstream isolator was shown to provide almost complete damping of pressure disturbances propagating upstream from the CDC towards the compressor.

Further efforts will be directed towards transition from hydrogen to liquid hydrocarbon fuel and the design of a downstream isolator protecting the turbine from pressure disturbances generated in the CDC.

## ACKNOWLEDGMENTS

This work was partly supported by the Russian Academy of Sciences (Program #26 “Combustion and Explosion”), Russian Foundation for Basic Research (grant 15-08-00782), and Russian Science Foundation (grant 14-13-00082).

## REFERENCES

1. Zel'dovich, Ya. B. 1940. On utilizing detonative combustion in power engineering. *Sov. J. Techn. Phys.* 10(17):1453–1461.
2. Voitsekhovskii, B. V. 1959. Stationary detonation. *Dokl. USSR Acad. Sci.* 129:1254–1256.
3. Roy, G. D., S. M. Frolov, A. A. Borisov, and D. W. Netzer. 2004. Pulse detonation propulsion: Challenges, current status, and future perspective. *Prog. Energy Combust. Sci.* 30(6):545–672.
4. Frolov, S. M., ed. 2006. *Pulse detonation engines*. Moscow: TORUS PRESS. 592 p.
5. Bykovskii, F. A., S. A. Zhdan, and E. F. Vedernikov. 2006. Continuous spin detonation of fuel–air mixtures. *Combust. Explor. Shock Waves* 42(4):1–9.
6. Bykovskii, F. A., S. A. Zhdan, and E. F. Vedernikov. 2010. Continuous spin detonation of a hydrogen–air mixture with addition of air into the products and the mixing region. *Combust. Explor. Shock Waves* 46(1):52–59.
7. Davidenko, D. M., I. Gokalp, and A. N. Kudryavtsev. 2008. Numerical study of the continuous detonation wave rocket engine. AIAA Paper No. 2008-2680.

8. Hishida, M., T. Fujiwara, and P. Wolanski. 2009. Fundamentals of rotating detonations. *Shock Waves* 19(1):1–10.
9. Shao, Y.-T., M. Liu, and J.-P. Wang. 2010. Numerical investigation of rotating detonation engine propulsive performance. *Combust. Sci. Technol.* 182:1586–1597.
10. Kindracki, J., P. Wolanski, and Z. Gut. 2011. Experimental research on the rotating detonation in gaseous fuels–oxygen mixtures. *Shock Waves* 21(2):75–84.
11. Frolov, S. M., A. V. Dubrovskii, and V. S. Ivanov. 2012. Three-dimensional numerical simulation of the operation of the rotating detonation chamber. *Russ. J. Phys. Chem. B* 6(2):276–288.
12. Tchvanov, V. K., S. M. Frolov, and E. L. Sternin. 2012. Liquid-fueled rocket detonation engine. *Trans. NPO Energomash* 29:4–14.
13. Schwer, D., and K. Kailasanath. 2013. Fluid dynamics of rotating detonation engines with hydrogen and hydrocarbon fuels. *Proc. Combust. Inst.* 34(2):1991–1998.
14. Frolov, S. M., A. V. Dubrovskii, and V. S. Ivanov. 2013. Three-dimensional numerical simulation of operation process in rotating detonation engine. *Progress in propulsion physics*. Eds. L. DeLuca, C. Bonnal, O. Haidn, and S. Frolov. EUCASS advances in aerospace sciences book ser. EDP Sciences–TORUS PRESS. 4:467–488.
15. Frolov, S. M., A. V. Dubrovskii, and V. S. Ivanov. 2013. Three-dimensional numerical simulation of the operation of a rotating-detonation chamber with separate supply of fuel and oxidizer. *Russ. J. Phys. Chem. B* 7(1):35–43.
16. Frolov, S. M., A. V. Dubrovskii, and V. S. Ivanov. 2013 (submitted). The way of arranging the operation process in the continuous detonation chamber for gas turbine engine and the device for its implementation. Patent of Russian Federation.
17. Pope, S. B. 1985. PDF methods for turbulent reacting flows. *Prog. Energy Combust. Sci.* 11:119–192.
18. Frolov, S. M., and V. S. Ivanov. 2010. Combined flame tracking–particle method for numerical simulation of deflagration-to-detonation transition. *Deflagrative and detonative combustion*. Eds. G. Roy and S. Frolov. Moscow: TORUS PRESS. 133–156.
19. Ivanov, V. S., and S. M. Frolov. 2011. Numerical simulation of the operation process and thrust performance of an air-breathing pulse detonation engine in supersonic flight conditions. *Russ. J. Phys. Chem. B* 5:597–609.
20. Frolov, S. M., V. S. Ivanov, B. Basara, and M. Suffa. 2013. Numerical simulation of flame propagation and localized preflame autoignition in enclosures. *J. Loss Prevention Proc. Ind.* 26:302–309.
21. Basevich, V. Ya., and S. M. Frolov. 2007. Kinetics of blue flames in the gas-phase oxidation and combustion of hydrocarbons and their derivatives. *Russ. Chem. Rev.* 76(9):867–884.
22. Frolov, S. M., S. N. Medvedev, V. Ya. Basevich, and F. S. Frolov. 2013. Self-ignition of hydrocarbon–hydrogen–air mixtures. *Int. J. Hydrogen Energy* 38:4177–4184.